Hindawi Publishing Corporation
Journal of Nanomaterials
Volume 2012, Article ID 571015, 9 pages
doi:10.1155/2012/571015

Research Article

Contrast Enhancement of Optical Coherence Tomography Images Using Branched Gold Nanoparticles

Y. Ponce de León, J. L. Pichardo-Molina, N. Alcalá Ochoa, and D. Luna-Moreno

Photonics Division, Centro de Investigaciones en Óptica, A. C. Loma del Bosque 115, Col. Lomas del Campestre, 37150 León, GTO, Mexico

Correspondence should be addressed to J. L. Pichardo-Molina, jpichardo@cio.mx

Received 7 August 2012; Revised 29 September 2012; Accepted 12 October 2012

Academic Editor: Shuangxi Xing

We propose the use of branched gold nanoparticles (B-GNPs) as a contrast agent for optical coherence tomography (OCT) imaging. Our results show that even when the central source of our OCT (1325 nm) is too far from the maximum peak of the plasmon resonance, branched nanoparticles scatter light very efficiently at this wavelength. B-GNPs were tested as a contrast agent in water and agarose-TiO_2 tissue phantoms; the estimated increments in contrast were 9.19 dB and 15.07 dB for branched nanoparticles in water with concentrations of 2.2×10^9 NPs/mL and 6.6×10^9 NPs/mL, respectively, while for agarose-TiO_2 tissue phantoms the estimated value was 3.17 dB. These results show the promising application of B-GNPs as a contrast agent for tissue imaging using OCT, not only for sources at 1325 nm but also at other central wavelengths located between 800 and 1000 nm.

1. Introduction

Different endogenous materials have been investigated as contrast agents in optical coherence tomography imaging of tissue structure [1–5]; however, they are very expensive, exhibit low photostability values, introduce poor contrast enhancement, and are difficult to tune in the NIR region. In the last decade, new materials, such as metallic and polymeric nanoparticles (NPs), have been designed to have very interesting optical properties [6–8], but few have been explored as contrast agents [9–14]. Metallic NPs have many advantages over dyes and polymeric nanomaterials; they show high photostability and their plasmon band is easily tuned from visible to NIR by controlling their size and morphology [15–17]. The electric field near the nanoparticle surface can be highly amplified by the plasmon resonance, which is principally used in surface-enhanced Raman scattering (SERS). Resonant excitation of plasmons also contributes to the strong sensitivity of plasmon resonance to the local dielectric environment, which is exploited in localized surface plasmon resonance (LSPR) sensing [18]. Nonlinear optical effects are also present, such as second harmonic generation (SHG) [19, 20]. Additionally, gold NPs are biocompatible and nontoxic, and they can be functionalized to target specific biomarkers of tissue and cells [21–23].

Nanoparticles of different morphologies, such as nanospheres, nanocages, or nanorods, have been used to increase the contrast of OCT images; however, the reports show that those geometries and sizes do not significantly improve contrast when the central wavelength of the OCT does not perfectly match the plasmon band of NPs. For example, Agrawal et al. [24] tested core/shell NPs of silica/gold with different sizes of core and shell; their NPs were tested in water and turbid tissue phantoms, getting the maximum enhancement for those NPs with a core of 291 nm and a shell of 25 nm (1.0×10^9 nanoshells/mL) for an OCT system with a central wavelength at 1300 nm. Cang et al. [12] fabricated gold nanocages of 35 nm with a plasmon band located at 716 nm, which match the spectrum of their OCT system; they tested the nanocages in a gelatin phantom embedded with TiO_2, and the tissue phantom was well contrasted due to strong light absorption by the nanocages. Another interesting work

was reported by Troutman et al. [11], who used gold nanorods of 80 and 120 nm in length with longitudinal plasmon bands located at 750 and 912 nm, respectively, they tested the gold nanorods in polyacrylamide tissue phantoms embedded with polystyrene nanospheres, and found that nanorods, which match the central wavelength of the OCT (890 nm), allow getting maximum enhancement of backscattered light, although out of this wavelength, enhancement is very low.

Recently, new exotic morphologies of metallic NPs have been synthesized; particularly those with tips, such as nanostars or branched nanoparticles [26–28], concave nanocubes [29], or nanoflowers [30]. These intricate morphologies exhibit strong light scattering at longer wavelengths (NIR) and have relatively small sizes. New synthesis methodologies open the viability of producing them with high reproducibility, thus making them suitable as contrast agents for OCT imaging.

To our knowledge, this is the first time that B-GNPs are reported to be used as a contrast agent for OCT imaging. Here, we present some results of the evaluation of B-GNPs in water and turbid tissue phantoms of agarose with TiO_2. Our results show several advantages of the B-GNPs over those previously reported: our nanoparticles are smaller, and the plasmon band is easily tuned in the NIR. The Vis-NIR extinction spectra shows that B-GNPs still scatter light very efficiently at 1325 nm, enhancing the contrast of the OCT images, and could be used for different central wavelengths.

2. Experimental Section

2.1. Synthesis of Nanoparticles

2.1.1. Branched Gold Nanoparticles. B-GNPs were fabricated following a process that is slightly different to the typical synthesis of concave gold nanocubes [29]. Before initiating the synthesis, all glassware was cleaned in aqua regia and rinsed with plenty of water. First, a cetyltrimethylammonium chloride (CTAC) solution of 10 mL at 0.1 M was prepared, to which, once it was well dissolved in Millipore water, 250 μL of $HAuCl_4$ (0.01 M) and 600 μL of freshly solution of $NaBH_4$ (0.01 M, prepared in an ice bath) were added; the colloid was prepared under continuous magnetic stirring. After $NaBH_4$ was added, the solution took a pale brown color. We continued the stirring for a couple of minutes, and then the colloid was left to stand for three hours. According to the transmission electron microscopy (TEM) images, the seed colloid consisted of spherical particles with a mean size of 4 ± 0.8 nm and with a typical concentration of $\approx 7.2 \times 10^{13}$ NPs/mL; see Table 1 for more details.

Once the gold seeds were ready, branched nanoparticles were prepared in the following way: solutions of 10 mL CTAC (0.1 M) were prepared under magnetic stirring, and, successively, 500 μL of $HAuCl_4$ (0.01 M), 100 μL of $AgNO_3$ (0.01 M), 200 μL of HCl (1 M), and 100 μL of ascorbic acid (0.1 M) were added. Finally, to initiate the growth of branched nanoparticles, 10 μL of diluted seeds at a rate of 1 : 100 in CTAC (0.1 M) were added. Magnetic stirring continued for 90 more minutes, and then the solution was left to stand undisturbed overnight.

2.1.2. Gold Nanospheres. Gold nanospheres were prepared following the Turkevich method reported elsewhere [31]. In a typical synthesis, 20 mL of water and 40 μL of $HAuCl_4$ (0.25 M) were added to a glass flask of 50 mL. The solution was heated to boiling point; then 300 μL of sodium citrate at 1% were added under continuous magnetic stirring. The solution changed from being transparent to violet, and finally it became ruby red.

2.1.3. Gold Nanorods. Gold nanorods were prepared using a seed-mediated method [32, 33]. First, the growth solution was prepared as follows: 5 mL of CTAB (0.2 M), 5 mL of $HAuCl_4$ (0.5 mM), and 600 μL of $NaBH_4$ (0.01 M) were mixed to get the growth solution, which was used as seeds within 1-2 hours after preparation; once the seeds were ready, we proceeded to prepare the gold nanorods. In a typical synthesis procedure, 10 mL of CTAB (0.2 M) and 10 mL of $HAuCl_4$ (0.5 mM) were added to a 50 mL glass flask, all under magnetic stirring; then, 220 μL of $AgNO_3$ (1 mM) and 95 μL of ascorbic acid (0.1 M) were added to get a transparent solution. Finally, 12 μL of the seed solution were added. Magnetic stirring continued for five more minutes, and, then, the solution remained undisturbed overnight.

2.2. Vis-NIR Spectroscopy and TEM Analysis. The B-GNPs, nanospheres, and nanorods that were obtained were analyzed by means of Vis-NIR spectroscopy and transmission electron microscopy. Extinction spectra of the colloids were acquired using a Perkin Elmer lambda 900 spectrometer, with a spectral resolution of ± 0.08 nm for UV/Vis and ± 0.30 nm for NIR. The top graph of Figure 1 shows the Vis-NIR optical extinction spectrum of B-GNPs recorded with a concentration of $\approx 6.6 \times 10^9$ NPs/mL; the spectrum is represented by the continuous line. The maximum peak of the extinction spectrum is located at 765 nm, but a deconvolution analysis shows that it can be described by four Gaussian peaks represented by the symbols $\star$, $\blacksquare$, $+$ and $\circ$ (see Figure 1). The first peak ($\star$) is located at 555 nm and corresponds to the size of the core of the B-GNPs, while the other three peaks may correspond to the plasmon hybridization of the tips with the core [18]. In fact, the last two peaks are located in the NIR, and the central wavelength of the source of the OCT is close to resonance with the last peak at 1198 nm. The bottom graph of Figure 1 shows the absorption spectra corresponding to nanospheres (continuous line) and nanorods (dotted line); the maximum absorption peak for nanospheres is located at 570 nm, while the absorption peaks for nanorods are, respectively, located at 519 and 764 nm for the transversal and longitudinal plasmon bands.

Several authors, like Kumar et al. [34] and Trigari et al. [35], have reported the modeling of gold nanostars with tunable morphology. NPs with large tips display a significant shift of the plasmon band to the NIR region.

For our case, the mean size and the geometrical shape of B-GNPs, nanospheres, and nanorods were determined by

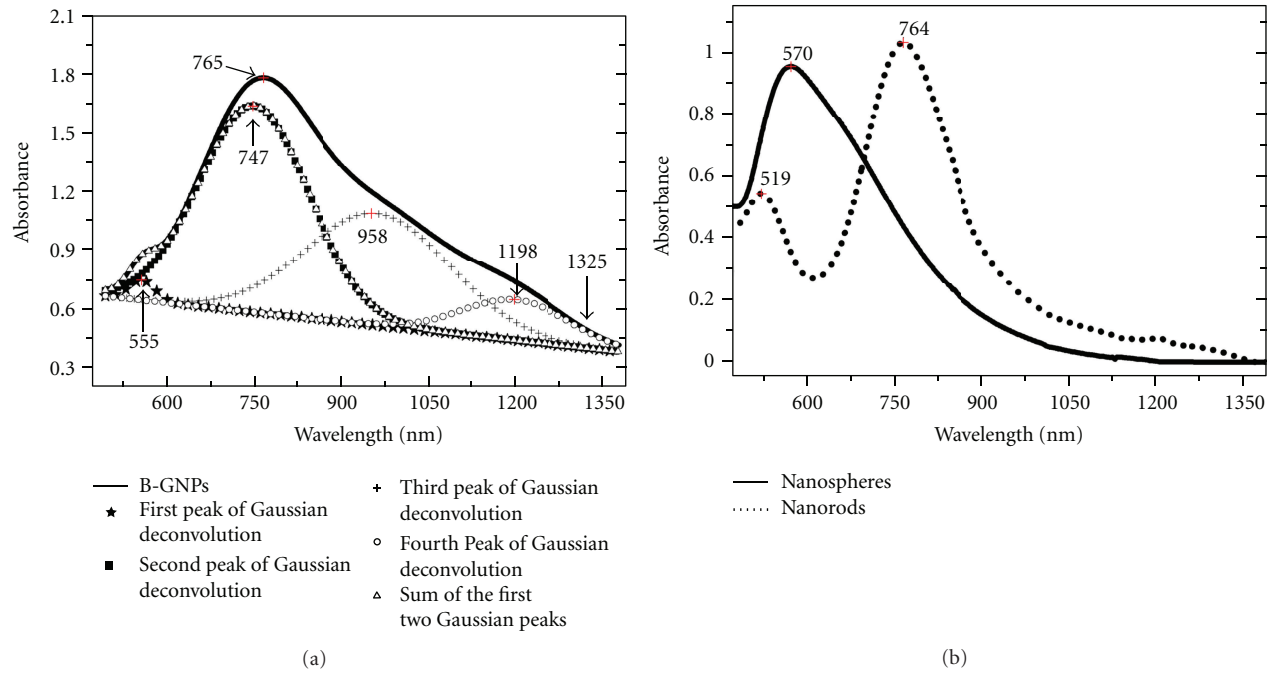

Figure 1: (a) corresponds to the absorption spectrum of B-GNPs and their Gaussian deconvolution. The continuous line corresponds to the Vis-NIR extinction spectrum of branched gold nanoparticles, while the next four curves correspond to the Gaussian deconvolution. The last curve represented by △ symbols corresponds to the sum of peaks one and two (⋆ and ■). (b) corresponds to the absorption spectra of nanospheres and nanorods.

Table 1: Summary of gold seeds and B-GNPs.

Seed concentration (no. of seeds/mL)	Mean core size of B-GNPs (nm)	Mean tip length of B-GNPs (nm)	Concentration[a] (no. of B-GNPs/mL)
7.2×10^{13}	78 ± 13	40 ± 15	6.6×10^{9}

[a]NP concentration was calculated in a manner similar to that in reference [25].

TEM (Philips, MORGAGNI 268); Figure 2 shows the characteristic TEM images of branched NPs, nanospheres, and nanorods. After a careful analysis carried out in several TEM images using the ImageJ software 1.42q (Wayne Rasband National Institutes of Health, USA), for B-GNPs we measured a mean core size of 78 ± 13 nm and a mean length size of 40 ± 15 nm for their tips; nonetheless, it is possible to find a few B-GNPs with tips of 120 nm of length. For nanospheres, the mean diameter was 64 ± 12 nm, and for nanorods the mean length and diameter were 44 ± 5 nm and 11 ± 1 nm, respectively. Additional information related to the seeds and B-GNPs is shown in Table 1.

2.3. Gel Samples Preparation and OCT System. To evaluate the efficiency of B-GNPs as a contrast agent for OCT imaging, our NPs were tested in water and agarose-TiO_2 tissue phantoms. Agarose-TiO_2 phantoms were prepared in the following way: 0.1 g of agarose and 10 mg of TiO_2 were added to 10 mL of water at boiling point, all under magnetic stirring. Previously, 20 μL of concentrated NPs had been obtained from the centrifugation (1500 rpm, 10 min) of 1.5 mL of NPs solution; the NPs were then sonicated for ten minutes, and, afterwards, 30 μL of agarose gel were added. A three-layer phantom was prepared as follows: first, one layer was prepared with agarose-TiO_2 solution; after that layer gelled, the agarose solution with NPs (1.9×10^{11} NPs/mL) was poured over it, and, finally, the solution of agarose-TiO_2 was poured to form the last layer. The tissue phantom was analyzed with a Swept Source Optical Coherence Tomography Imaging System (Thorlabs OCS1300SS) at a central wavelength of 1325 nm, with a spectral bandwidth of 100 nm.

3. Results and Discussion

B-GNPs were studied as a contrast agent for OCT imaging in water and agarose-TiO_2 tissue phantom. To show the efficiency of our B-GNPs, we compared them with other morphologies, such as nanorods and nanospheres. Figure 3 shows the OCT B-scan images corresponding to water samples with nanospheres, nanorods, and B-GNPs, while Figure 4 shows the OCT B-scan image of the agarose-TiO_2 tissue phantom with B-GNPs; in both cases, the air-water and air-phantom interfaces can be identified because the border of the interface looks very bright at the top of each image. Also, for all water images, a white line, a little below

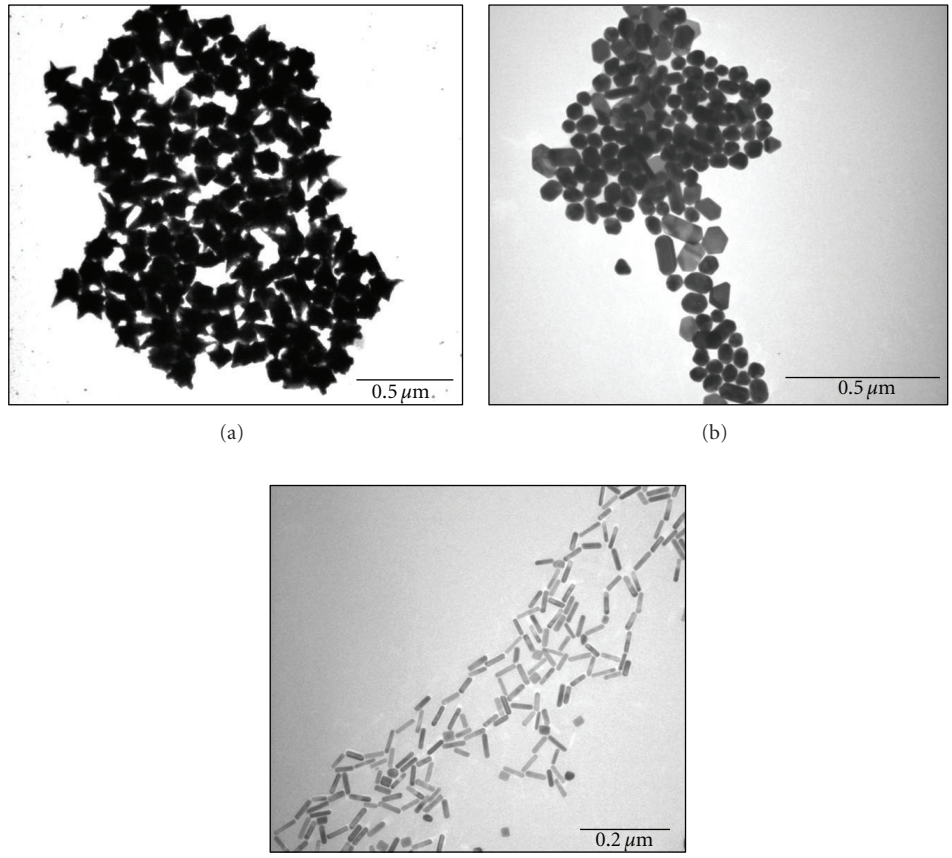

(a) (b)

(c)

Figure 2: TEM images of (a) B-GNPs with mean core diameter of 78 ± 13 nm and mean tip length of 40 ± 15 nm, (b) nanospheres with mean diameter of 64 ± 12 nm, and (c) nanorods with mean length and diameter of 44 ± 5 and 11 ± 1 nm, respectively.

the interface, was drawn as reference for future calculations of the average A-scan profiles and for quantitative contrast enhancement calculations.

Figure 3(a) shows the OCT B-scan image for the case of Millipore water (18.2 MΩcm and <10 ppb total organic carbon). The OCT image of water is poorly contrasted due to the low intensity of the scattered light; it is difficult to appreciate any bright spot from water molecules, and excepting the interface, the image is almost totally black. Something similar happens in the case of nanorods (2.1×10^{12} NPs/mL) (see Figure 3(b)): contrast is very poor, except for a few bright spots which can be attributed to big nanoparticles. On the other hand, in the case of nanospheres (see Figure 3(c)), contrast is notably improved, but it still shows weak contrast enhancement of the image, in spite of the concentration of nanospheres (3.7×10^{10} NPs/mL) being higher than that of the diluted B-GNPs. These results can be explained from the absorption spectra of nanorods and nanospheres; optical extinction around 1325 nm is almost zero, so we cannot expect high contrast enhancement due to low scattering intensity. However, for B-GNPs prepared at a concentration of $\approx 2.2 \times 10^9$ NPs/mL, the intensity due to scattering becomes very strong (see Figure 3(d)). The cross-sectional image of water with B-GNPs shows spots of similar sizes but with significant differences in intensity. These changes in intensity mean that some of these particles scatter light more efficiently at the central wavelength of the OCT source. In theory, each spot corresponds to one nanoparticle, although we do not discard the possibility of a low degree of aggregation which also produces a very efficient process of scattering. As a matter of fact, we expect that the brightest spots correspond to B-GNPs with larger tips. In fact, OCT images of water with B-GNPs were acquired with a concentration of 6.6×10^9 NPs/mL (see Figure 3(e)), but this time we could not see the isolated spots corresponding to each nanoparticle, and we only appreciate a bright continuous background, due to the high concentration of NPs. The characteristic mean A-scan was calculated averaging a total of 512 A-scans for the different cases: water without NPs, nanospheres in water, nanorods in water, and diluted and nondiluted B-GNPs in water (see Figure 3(f)). Again, from these profiles, we can more clearly see the high efficiency of B-GNPs to enhance the contrast of OCT images. The profile corresponding to water is very flat, as is the nanorods profile, while the profile for nanospheres has a similar intensity of diluted B-GNPs,

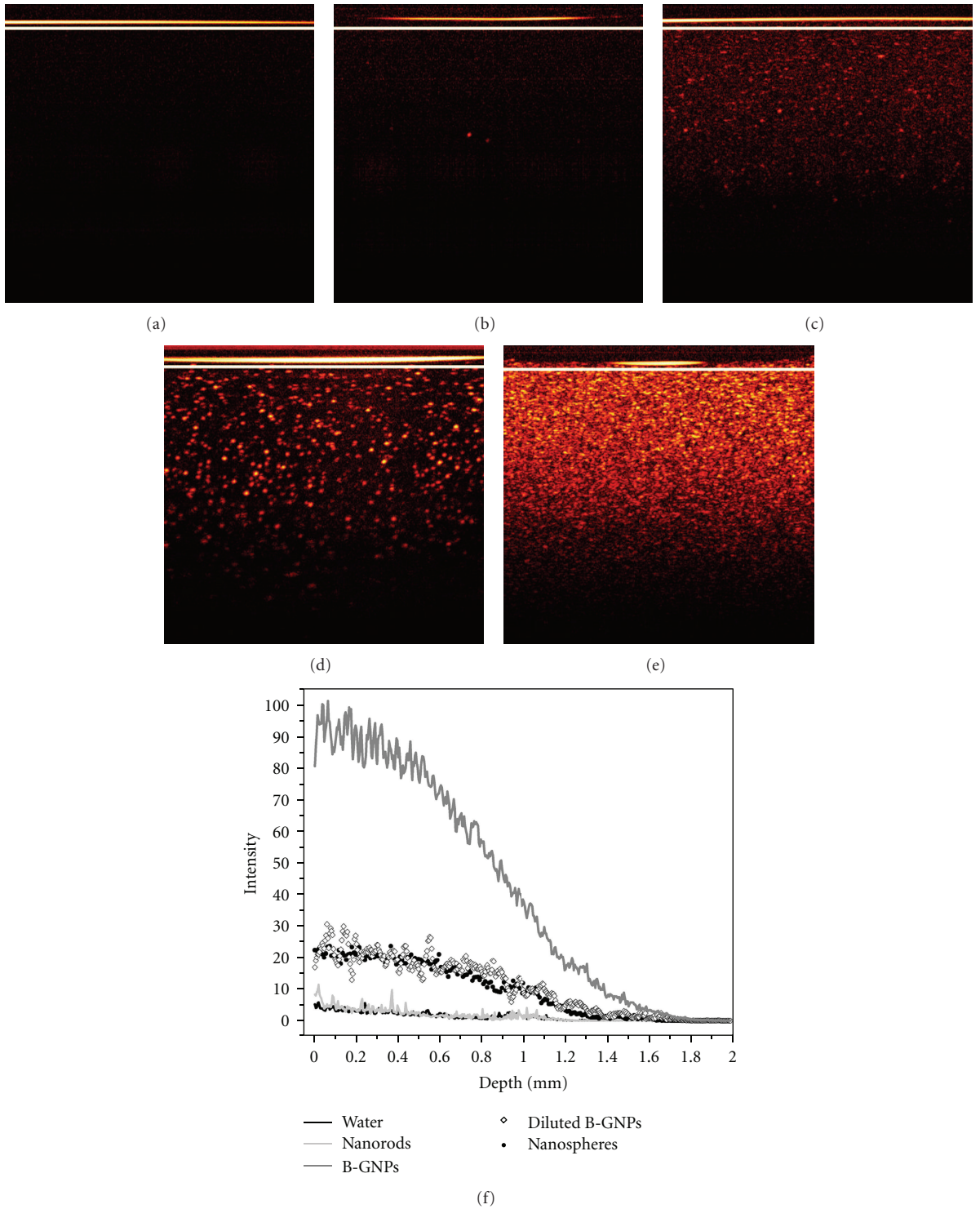

Figure 3: OCT B-scan images of (a) water without NPs, (b) nanorods in water, (c) nanospheres in water, (d) diluted B-GNPs in water, (e) B-GNPs in water, and (f) average A-scan profiles of the water samples. Water without NPs is represented by the black continuous line, nanorods in water by the light gray continuous line, nanospheres in water by •, diluted B-GNPs by ◊, and B-GNPs by the gray continuous line.

showing that B-GNPs are more efficient than nanospheres to enhance the contrast of OCT images. On the other hand, B-GNPs without dilution show a very high intensity increment in comparison with the other nanoparticles; indeed, the reflected light intensity at 0.2 mm of depth is around four times higher than that for nanospheres.

The main goal of the present work is to show the usefulness of the B-GNPs as a contrast agent for tissue analysis

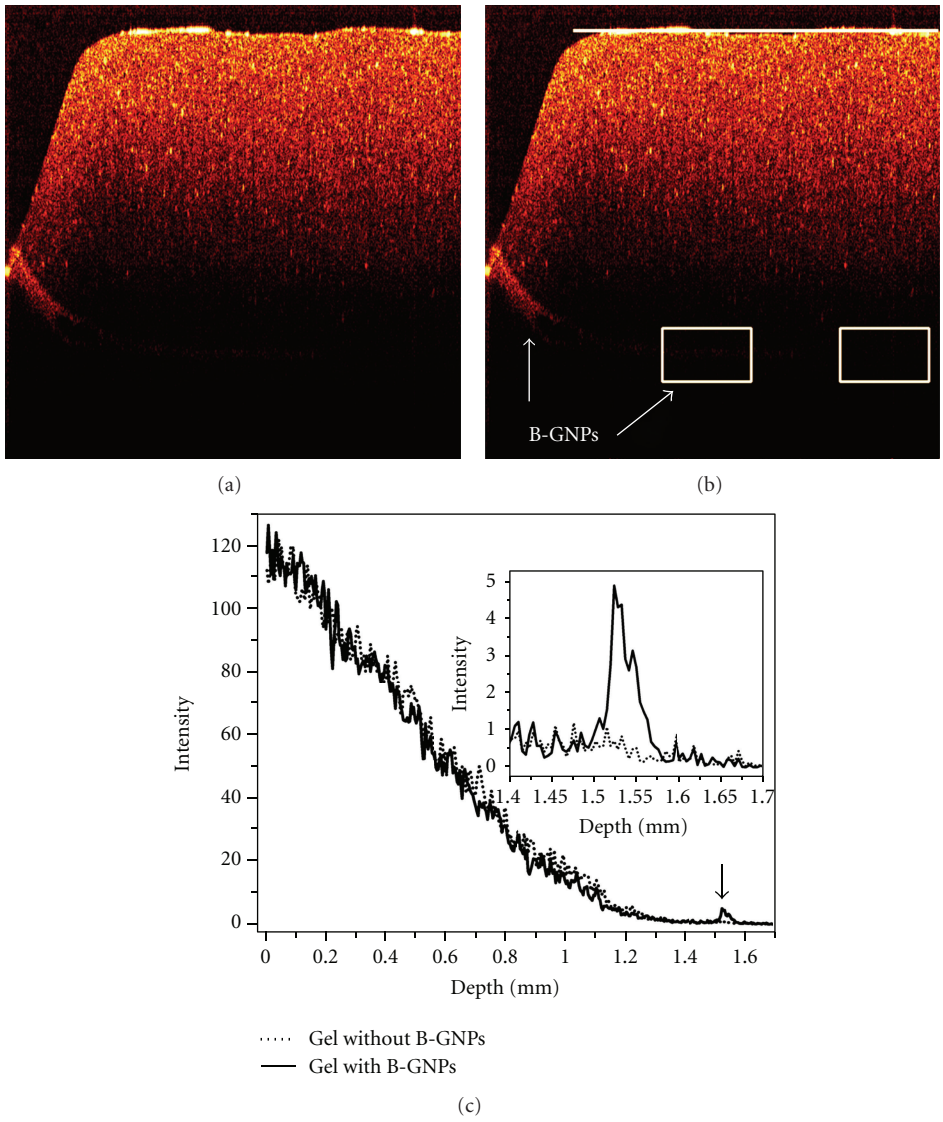

Figure 4: (a) Characteristic OCT B-scan image of tissue phantom with and without B-GNPs. (b) OCT B-scan image of tissue phantom showing the corresponding zones used to calculate contrast enhancement (white squares). (c) Average A-scan of tissue phantom without B-GNPs is represented by the dotted line, while average A-scan of tissue phantom with B-GNPs is represented by the continuous line. Inset: zoom of the profile corresponding to the depth of the layer with nanoparticles (signaled by the arrow) showing the enhancement of backscattered light.

(enhancing the contrast of OCT images of tissue layers); for this reason, we analyzed the simulated turbid tissue phantoms of agarose-TiO_2 with and without B-GNPs. Figure 4(a) shows the OCT B-scan image of the turbid tissue phantom; remember that our phantom was prepared with B-GNPs (1.9×10^{11} NPs/mL) on the left, but without NPs on the right.

At the bottom of the right side of Figure 4(a), the OCT image shows the tissue phantom without B-GNPs; the contrast of the image in this zone is very poor due to the fact that the intensity of backscattered light is very low at this depth, $\approx$1.5 mm. On the other hand, at the bottom of the left side, at the same depth, a thin bright layer can be noticed, which corresponds to a thin layer of agarose with B-GNPs. The arrows in Figure 4(b) show the location of the B-GNPs.

After careful visual inspection, it can be observed that the OCT image displays significant variation in intensity of backscattered light along the layer of B-GNPs, since the upper layer of agarose-TiO_2 on the left side is thinner than on the right side; indeed, the left side shows the presence of an air bubble in the phantom, and the air bubble sent the NPs outside. Then, the NPs around the bubble show good contrast enhancement when compared to the area inside the bubble. Figure 4(c) shows the average profile of the tissue phantom for both cases: the dotted line represents the phantom without B-GNPs, while the continuous line represents the profile of the phantom with branched NPs. The average profile of the tissue phantom without B-GNPs shows a relatively smooth curve. In fact, no abrupt changes of intensity

Table 2: Summary of average pixel intensities and contrast enhancement values.

Sample	Average pixel intensity	Contrast enhancement (dB)
Water without NPs	1.30	—
B-GNPs in water	41.91	15.07
Diluted B-GNPs in water	10.81	9.19
Nanospheres in water	9.72	8.72
Nanorods in water	1.51	0.65
Gel with TiO_2 with B-GNPs	0.91	3.17
Gel with TiO_2 without B-GNPs	0.44	—

can be appreciated, as it was observed in the profile of water with NPs, which means that the TiO_2 in the phantom was distributed very homogeneously. Also, it can be noticed that the backscattering light decreases continuously as a function of depth. A similar behavior is observed for the case where B-GNPs were used, except at the depth of 1.52 mm, where a sharp peak of backscattered light is observed. This peak shows that even though our nanoparticles are smaller than the TiO_2 particles, they are more efficient at backscattering light.

In order to get a more quantitative and reliable analysis of the behavior of our B-GNPs, the quantification of the contrast enhancement for OCT images was calculated using the following equation *10 *log10 (average pixel intensity of the area with NPs/average pixel intensity of the reference area)* [11]. In all cases (water with nanoparticles), we considered an area of 2.00 mm × 1.98 mm for contrast enhancement calculation; the area was selected just below the air-water interface (white line), where our reference was a sample of Millipore water. The estimated increments in contrast were 9.19 dB for diluted B-GNPs in water and 15.07 dB for nondiluted B-GNPs. As we have mentioned, a similar procedure was carried out with the gold nanorods and nanospheres at the concentrations given above; the results for contrast enhancement were 0.65 and 8.72 dB, respectively. From these results, we observed that even though nanorods show the plasmon band at 764 nm, almost at the same position of B-GNPs; contrast enhancement is very poor in this case. On the other hand, gold nanospheres show good contrast enhancement, almost the same that was obtained for diluted B-GNPs nanoparticles; however, for nondiluted B-GNPs, contrast enhancement is 1.7 times greater than that for nanospheres, which have a concentration (NPs/mL) one order of magnitude greater than B-GNPs. These results mean that B-GNPs work very well as a contrast agent in water, and that their performance is better than the one seen in the other two cases. Consequently, B-GNPs are the best option to use as a contrast agent in tissue phantoms in order to produce good optical contrast enhancement of OCT images.

Following a procedure similar to the one used with water samples, the contrast enhancement of agarose-TiO_2 tissue phantoms with NPs was calculated. For this case, we selected a rectangular area of 1.95 mm × 0.26 mm (see Figure 4(b)); the white square on the left corresponds to tissue phantom with NPs, and the average pixel intensity of the area with NPs was obtained from this square, while the white square on the right corresponds to the tissue phantom without NPs, from which we calculated the average pixel intensity of the reference area. The calculated contrast enhancement using the above equation is equivalent to 3.17 dB. See Table 2 for more details.

The present results show that the geometrical shape of branched NPs, which tune the plasmon resonance band at NIR, still enhances the backscattering light of the central wavelength of the OCT at 1325 nm very efficiently. Additionally, the optical extinction spectrum predicts that B-GNPs can be used as a contrast agent for OCT imaging with central sources close to 800 and 900 nm, unlike core/shell, nanocages, or nanorods, which generally match just one of these central wavelength sources. The main reason is the behavior of the spectral extinction of the B-GNPs; as it has been shown, they exhibit three interesting peaks, located at 747, 958, and 1198 nm, that can be close to resonance with different OCT sources.

4. Conclusions

To our knowledge, this is the first time that B-GNPs are reported to be used as a contrast agent in OCT imaging. In the present work, we have proposed the use of branched gold NPs with a suitable mean core size of 78 nm and a mean tip length of 40 nm; as it has been mentioned, they exhibit three interesting peaks, located at 747, 958, and 1198 nm, that can be close to resonance with different central sources used for OCT imaging, yielding a very strong interaction with the plasmon resonance and enhancing backscattered light, unlike nanorods, which only match one central wavelength, or nanospheres, which scatter light only if their size is big (bulk effect).

Our B-GNPs were evaluated in water and agarose-TiO_2 tissue phantoms, obtaining very good contrast enhancement: 9.19 dB for the case of B-GNPs diluted in water, 15.07 dB for the non-diluted sample, and 3.17 dB for agarose-TiO_2 tissue phantoms.

In general, we obtained considerable good increments in the contrast of images, indicating that even though the maximum peak of the plasmon band is far away from the central wavelength of the OCT system, the peak located at 1198 nm is an indication that B-GNPs are still very efficient at scattering light at this wavelength. So, B-GNPs can be considered a good contrast agent for OCT imaging.

Acknowledgments

Authors would like to thank the financial support of CONACyT under Grants no. 152971 and 133495, and CONACyT & DTS 164203. They thank Mario Ruiz for his contribution to English grammar review and Enrique N. Arias, Martin Olmos, and Aurora Verver for their technical assistance. They also thank the reviewers for their valuable comments towards the improvement of the paper.

References

[1] C. Yang, "Molecular contrast optical coherence tomography: a review," *Photochemistry and Photobiology*, vol. 81, no. 2, pp. 215–237, 2005.

[2] C. Xu, J. Ye, D. L. Marks, and S. A. Boppart, "Near-infrared dyes as contrast-enhancing agents for spectroscopic optical coherence tomography," *Optics Letters*, vol. 29, no. 14, pp. 1647–1649, 2004.

[3] C. Yang, M. A. Choma, L. E. Lamb, J. D. Simon, and J. A. Izatt, "Protein-based molecular contrast optical coherence tomography with phytochrome as the contrast agent," *Optics Letters*, vol. 29, no. 12, pp. 1396–1398, 2004.

[4] C. Yang, L. E. L. McGuckin, J. D. Simon, M. A. Choma, B. E. Applegate, and J. A. Izatt, "Spectral triangulation molecular contrast optical coherence tomography with indocyanine green as the contrast agent," *Optics Letters*, vol. 29, no. 17, pp. 2016–2018, 2004.

[5] N. Iftimia, A. K. Iyer, D. X. Hammer et al., "Fluorescence-guided optical coherence tomography imaging for colon cancer screening: a preliminary mouse study," *Biomedical Optics Express*, vol. 3, no. 1, pp. 178–191, 2012.

[6] M. Pelton, J. Aizpurua, and G. Bryant, "Metal-nanoparticle plasmonics," *Laser and Photonics Reviews*, vol. 2, no. 3, pp. 136–159, 2008.

[7] M. Rycenga, C. M. Cobley, J. Zeng et al., "Controlling the synthesis and assembly of silver nanostructures for plasmonic applications," *Chemical Reviews*, vol. 111, no. 6, pp. 3669–3712, 2011.

[8] N. J. Halas, S. Lal, W. S. Chang, S. Link, and P. Nordlander, "Plasmons in strongly coupled metallic nanostructures," *Chemical Reviews*, vol. 111, no. 6, pp. 3913–3961, 2011.

[9] E. V. Zagaynova, M. V. Shirmanova, M. Y. Kirillin et al., "Contrasting properties of gold nanoparticles for optical coherence tomography: phantom, in vivo studies and Monte Carlo simulation," *Physics in Medicine and Biology*, vol. 53, no. 18, pp. 4995–5009, 2008.

[10] Y. L. Kim, V. M. Turzhitsky, Y. Liu et al., "Low-coherence enhanced backscattering: a review of principles and applications for colon cancer screening," *Journal of Biomedical Optics*, vol. 11, no. 4, Article ID 041125, 2006.

[11] T. S. Troutman, J. K. Barton, and M. Romanowski, "Optical coherence tomography with plasmon resonant nanorods of gold," *Optics Letters*, vol. 32, no. 11, pp. 1438–1440, 2007.

[12] H. Cang, T. Sun, Z. Y. Li et al., "Gold nanocages as contrast agents for spectroscopic optical coherence tomography," *Optics Letters*, vol. 30, no. 22, pp. 3048–3050, 2005.

[13] S. A. Boppart, "Advances in contrast enhancement for optical coherence tomography," in *Proceedings of the 28th Annual International Conference of the IEEE Engineering in Medicine and Biology Society (EMBS '06)*, pp. 121–124, New York, NY, USA, September 2006.

[14] M. A. Hahn, A. K. Singh, P. Sharma, S. C. Brown, and B. M. Moudgil, "Nanoparticles as contrast agents for in-vivo bioimaging: current status and future perspectives," *Analytical and Bioanalytical Chemistry*, vol. 399, no. 1, pp. 3–27, 2011.

[15] M. Grzelczak, J. Pérez-Juste, P. Mulvaney, and L. M. Liz-Marzán, "Shape control in gold nanoparticle synthesis," *Chemical Society Reviews*, vol. 37, no. 9, pp. 1783–1791, 2008.

[16] T. K. Sau and A. L. Rogach, "Nonspherical noble metal nanoparticles: colloid-chemical synthesis and morphology control," *Advanced Materials*, vol. 22, no. 16, pp. 1781–1804, 2010.

[17] B. Wiley, T. Herricks, Y. Sun, and Y. Xia, "Polyol synthesis of silver nanoparticles: use of chloride and oxygen to promote the formation of single-crystal, truncated cubes and tetrahedrons," *Nano Letters*, vol. 4, no. 9, pp. 1733–1739, 2004.

[18] F. Hao, C. L. Nehl, J. H. Hafner, and P. Nordlander, "Plasmon resonances of a gold nanostar," *Nano Letters*, vol. 7, no. 3, pp. 729–732, 2007.

[19] K. Ozga, T. Kawaharamura, A. Ali Umar et al., "Second order optical effects in Au nanoparticle-deposited ZnO nanocrystallite films," *Nanotechnology*, vol. 19, no. 18, Article ID 185709, 2008.

[20] I. V. Kityk, J. Ebothé, I. Fuks-Janczarek et al., "Nonlinear optical properties of Au nanoparticles on indium-tin oxide substrate," *Nanotechnology*, vol. 16, no. 9, pp. 1687–1692, 2005.

[21] B. van de Broek, N. Devoogdt, A. D'Hollander et al., "Specific cell targeting with nanobody conjugated branched gold nanoparticles for photothermal therapy," *ACS Nano*, vol. 5, no. 6, pp. 4319–4328, 2011.

[22] R. Wilson, "The use of gold nanoparticles in diagnostics and detection," *Chemical Society Reviews*, vol. 37, no. 9, pp. 2028–2045, 2008.

[23] C. Ungureanu, R. Kroes, W. Petersen et al., "Light interactions with gold nanorods and cells: implications for photothermal nanotherapeutics," *Nano Letters*, vol. 11, no. 5, pp. 1887–1894, 2011.

[24] A. Agrawal, S. Huang, A. W. H. Lin et al., "Quantitative evaluation of optical coherence tomography signal enhancement with gold nanoshells," *Journal of Biomedical Optics*, vol. 11, no. 4, Article ID 041121, 2006.

[25] N. R. Jana, L. Gearheart, and C. J. Murphy, "Seeding growth for size control of 5–40 nm diameter gold nanoparticles," *Langmuir*, vol. 17, no. 22, pp. 6782–6786, 2001.

[26] S. Chen, Z. L. Wang, J. Ballato, S. H. Foulger, and D. L. Carroll, "Monopod, bipod, tripod, and tetrapod gold nanocrystals," *Journal of the American Chemical Society*, vol. 125, no. 52, pp. 16186–16187, 2003.

[27] M. Yamamoto, Y. Kashiwagi, T. Sakata, H. Mori, and M. Nakamoto, "Synthesis and morphology of star-shaped gold nanoplates protected by poly(N-vinyl-2-pyrrolidone)," *Chemistry of Materials*, vol. 17, no. 22, pp. 5391–5393, 2005.

[28] O. M. Bakr, B. H. Wunsch, and F. Stellacci, "High-yield synthesis of multi-branched urchin-like gold nanoparticles," *Chemistry of Materials*, vol. 18, no. 14, pp. 3297–3301, 2006.

[29] J. Zhang, M. R. Langille, M. L. Personick, K. Zhang, S. Li, and C. A. Mirkin, "Concave cubic gold nanocrystals with high-index facets," *Journal of the American Chemical Society*, vol. 132, no. 40, pp. 14012–14014, 2010.

[30] H. Li, Y. Yang, Y. Wang, W. Li, L. Bi, and L. Wu, "In situ fabrication of flower-like gold nanoparticles in surfactant-polyoxometalate-hybrid spherical assemblies," *Chemical Communications*, vol. 46, no. 21, pp. 3750–3752, 2010.

[31] J. Kimling, M. Maier, B. Okenve, V. Kotaidis, H. Ballot, and A. Plech, "Turkevich method for gold nanoparticle synthesis

revisited," *Journal of Physical Chemistry B*, vol. 110, no. 32, pp. 15700–15707, 2006.

[32] N. R. Jana, L. Gearheart, and C. J. Murphy, "Wet chemical synthesis of high aspect ratio cylindrical gold nanorods," *Journal of Physical Chemistry B*, vol. 105, no. 19, pp. 4065–4067, 2001.

[33] B. Nikoobakht and M. A. El-Sayed, "Preparation and growth mechanism of gold nanorods (NRs) using seed-mediated growth method," *Chemistry of Materials*, vol. 15, no. 10, pp. 1957–1962, 2003.

[34] P. S. Kumar, I. Pastoriza-Santos, B. Rodríguez-González, F. Javier García de Abajo, and L. M. Liz-Marzán, "High-yield synthesis and optical response of gold nanostars," *Nanotechnology*, vol. 19, no. 1, Article ID 015606, 2008.

[35] S. Trigari, A. Rindi, G. Margheri, S. Sottini, G. Dellepiane, and E. Giorgetti, "Synthesis and modelling of gold nanostars with tunable morphology and extinction spectrum," *Journal of Materials Chemistry*, vol. 21, no. 18, pp. 6531–6540, 2011.